Commun. Comput. Phys.
doi: 10.4208/cicp.OA-2024-0241

Vol. **38**, No. 4, pp. 923-952
October 2025

High–Order Spectral Simulation of Dispersive Two–Dimensional Materials

David P. Nicholls[1,*] and Tianyu Zhu[1]

[1] *Department of Mathematics, Statistics, and Computer Science, University of Illinois at Chicago, Chicago, IL 60607, USA.*

Received 7 October 2024; Accepted (in revised version) 4 June 2025

Abstract. Over the past twenty years, the field of plasmonics has been revolutionized with the isolation and utilization of two–dimensional materials, particularly graphene. Consequently there is significant interest in rapid, robust, and highly accurate computational schemes which can incorporate such materials. Standard volumetric approaches can be contemplated, but these require huge computational resources. Here we describe an algorithm which addresses this issue for nonlocal models of the electromagnetic response of graphene. Our methodology not only approximates the graphene layer with a surface current, but also reformulates the governing volumetric equations in terms of surface quantities using Dirichlet–Neumann Operators. We have recently shown how these surface equations can be numerically simulated in an efficient, stable, and accurate fashion using a High–Order Perturbation of Envelopes methodology. We extend these results to the nonlocal model mentioned above, and using an implementation of this algorithm, we study absorbance spectra of TM polarized plane–waves scattered by a periodic grid of graphene ribbons.

AMS subject classifications: 78A45, 65N35, 78B22, 35J05, 41A58

Key words: Two–dimensional materials, graphene, non–local current models, electromagnetic scattering, high–order spectral methods.

1 Introduction

Over the past twenty years, the field of plasmonics has been revolutionized with the isolation and utilization of two–dimensional materials, particularly graphene. Graphene is a single layer of carbon atoms arranged in a honeycomb lattice which has striking mechanical, chemical, and electronic properties [11, 13]. It was first isolated in 2004 [26] resulting in the awarding of the 2011 Nobel Prize to Geim [12] and Novoselov [32]. At this point the literature on graphene is so vast that it is impossible to describe even a fraction

---

*Corresponding author. *Email addresses:* `davidn@uic.edu` (D. P. Nicholls), `tzhu29@uic.edu` (T. Zhu)

of it here, however, we point the interested reader to the website maintained by *Nature* dedicated to the major developments in the field [24]. The authors have found the survey article of Bludov, Ferriera, Peres, and Vasilevskiy [2] and survey book of Goncalves and Peres [15] to be particularly helpful.

Among the many optical phenomena associated to graphene, the collective charge oscillations known as plasmons [17, 19] are distinguished. Recently, the dispersive, nonlocal properties of these graphene plasmons have generated interest in the engineering literature [6, 8, 20, 23, 45] and the object of this contribution is to initiate this study. In particular, we describe a novel algorithm, inspired by our previous work [30], for simulating the scattering returns by a periodic array of graphene strips which takes into account the effects of nonlocality. We point out that, in addition to the optical phenomena that we have mentioned above, graphene has become indispensable in applications as diverse as energy storage [37], drug delivery and tumor therapy [39], biomedical devices [42], strain sensors [21], and membranes [25].

Before beginning our description, we point out that among the many techniques for numerically simulating structures featuring graphene (or other two–dimensional materials), simply solving the volumetric Maxwell equations in either the time domain (e.g., the Time Domain Finite Difference method [43]) or frequency domain (e.g., the Finite Element Method [18]) are natural options [9]. Typically, the graphene is modeled with an effective permittivity supported in a *thin* layer, or as a surface current with an effective conductivity at the interface between two layers [16]. In either case, commercial black–box Finite Element Method (FEM) software such as COMSOL Multiphysics™ [5] is typically utilized, however, these simulations are quite costly due to their low–order accuracy and volumetric character.

In our recent contributions [29, 30] we described a method which overcomes these drawbacks by not only restating the frequency domain governing equations in terms of *interfacial* unknowns, but also describing a highly accurate, efficient, and stable High–Order Spectral (HOS) algorithm [14, 40, 41]. A feature of our algorithm is that, in order to close the system of equations, surface integral operators must be introduced which connect interface traces of the scattered fields (Dirichlet data) to their surface normal derivatives (Neumann data). Such Dirichlet–Neumann Operators (DNOs) have been widely used and studied in the simulation of linear wave scattering, e.g., interfacial formulations of scattering problems [27, 29–31].

The object of our study is the plasmonic response that can be generated by graphene and, as in many photonic devices, structural periodicity is one path. This can be accomplished in several ways, and in one of our earlier papers [29] we focused upon graphene deposited on a periodically corrugated grating. In this the height/slope of the corrugation *shape* was viewed as a perturbation parameter and the resulting High–Order Perturbation of Shapes (HOPS) scheme sought corrections to the trivially computed flat–interface, solid graphene configuration. However, it is much more common to create a structure with *flat* interfaces upon which periodically spaced ribbons of graphene are mounted. In the paper [30] we modeled this configuration by multiplying the (constant) current function by an *envelope* function which transitions between one (where the graphene is deposited) to zero (where graphene is absent). Our numerical procedure viewed this envelope function as a perturbation of the identity function, and we termed that scheme a High–Order Perturbation of Envelopes (HOPE) algorithm. Our purpose in this contribution is to extend these latter results to the case of a nonlocal model for the response of a graphene layer. As we shall show, as such a model introduces higher order derivatives to the governing equations, this is a *highly* non–trivial extension requiring significant theoretical and algorithmic generalizations of those found in [30].

Using our HOPE method we not only rigorously demonstrate that the scattered fields depend analytically upon the envelope perturbation parameter, but also show that the resulting numerical scheme is both robust and accurate, and extremely rapid in its execution. As with the algorithm specified in [30], due to the flat interfaces of this geometry, the relevant DNOs are reduced to simple Fourier multipliers which can be easily computed in Fourier space. This is to be contrasted to the case of corrugated interfaces from [29] where a stable and accurate HOPS scheme for their computation is highly non–trivial to design and implement.

The rest of the paper is organized as follows: In Section 2 we recall the governing equations of our model [29,30] for the response of a two–dimensional material mounted between two dielectrics. In Section 3 we describe our surface formulation of these equations, specializing to the patterned, flat–interface configuration in Section 3.1. We prescribe our HOPE methodology in Section 3.2. We state and prove our analyticity results in Section 4. We conclude with numerical results in Section 5, with a discussion of implementation issues in Section 5.1 and simulation of absorbance spectra in Section 5.2.

2 Governing equations

Following [29], the structure we consider is displayed in Fig. 1, a doubly layered, y–invariant medium with periodic interface shaped by $z=g(x)$, $g(x+d)=g(x)$. This interface separates two domains filled with dielectrics of permittivities ϵ_u in $S^u := \{z > g(x)\}$ and ϵ_w in $S^w := \{z < g(x)\}$, respectively. This is illuminated with time–harmonic (of dependence $\exp(-i\omega t)$) plane–wave radiation of incidence angle θ, frequency ω, and wavenumber $k_u = \sqrt{\epsilon_u}\omega/c_0$,

$$v^{\text{inc}} = e^{i(\alpha x - \gamma_u z)}, \quad \alpha = k_u \sin(\theta), \quad \gamma_u = k_u \cos(\theta).$$

As we detailed in [29], if we choose as unknowns, $\{u(x,z), w(x,z)\}$, the laterally quasiperiodic transverse components of either the electric (Transverse Electric–TE) or magnetic (Transverse Magnetic–TM) fields, then the governing equations in this two–layer configuration are

$$u - w + A\tau_w \partial_N w = \xi, \qquad z = g(x), \tag{2.1a}$$

$$\tau_u \partial_N u - \tau_w \partial_N w + Bw = \tau_u \nu, \quad z = g(x), \tag{2.1b}$$

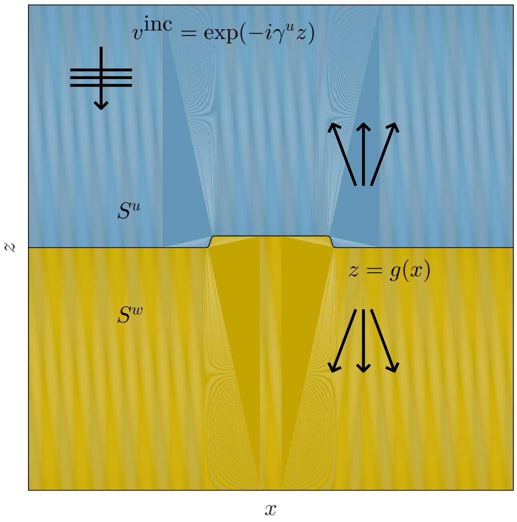

Figure 1: Plot of two–layer structure with periodic interface.

where $\partial_N = N\cdot\nabla$, $N = (-\partial_x g, 1)^T$,

$$\tau_m = \begin{cases} 1, & \text{TE}, \\ 1/\epsilon_m, & \text{TM}, \end{cases} \quad A = \begin{cases} 0, & \text{TE}, \\ |N|\hat{\sigma}/(ik_0), & \text{TM}, \end{cases} \quad B = \begin{cases} (ik_0)\hat{\sigma}/|N|, & \text{TE}, \\ 0, & \text{TM}, \end{cases}$$

for $m \in \{u,w\}$, and

$$\xi(x) = -\left. v^{\text{inc}} \right|_{z=g(x)}, \quad \nu(x) = -\left. \partial_N v^{\text{inc}} \right|_{z=g(x)}.$$

Of particular note is $\hat{\sigma} = \sigma/(\epsilon_0 c_0)$, the dimensionless *surface* current which models the effects of the graphene (or other two–dimensional material) deposited at the interface between the two layers.

3 Surface formulation

Following [27,29] we now reformulate the problem (2.1) in terms of surface integral operators, in this case Dirichlet–Neumann Operators (DNOs). For this we define the Dirichlet traces

$$U(x) := u(x, g(x)), \quad W(x) := w(x, g(x)),$$

and the outward pointing Neumann traces

$$\tilde{U}(x) := -(\partial_N u)(x, g(x)), \quad \tilde{W}(x) := (\partial_N w)(x, g(x)).$$

In terms of these (2.1) read

$$U-W+A\tau_w\tilde{W}=\xi, \tag{3.1a}$$

$$-\tau_u\tilde{U}-\tau_w\tilde{W}+BW=\tau_u\nu. \tag{3.1b}$$

These specify two equations for four unknowns which would be problematic except that U and $\tilde{U}$ are connected, as are W and $\tilde{W}$. We formalize this with the following definitions [28].

Definition 3.1. Given the unique quasiperiodic upward propagating solution [1] to

$$\Delta u+k_u^2u=0, \quad z>g(x), \tag{3.2}$$

subject to the Dirichlet condition, $u(x,g(x))=U(x)$, the Neumann data, $\tilde{U}(x)$, can be computed. The DNO G is defined by

$$G(g):U\to\tilde{U}.$$

Definition 3.2. Given the unique quasiperiodic downward propagating solution [1] to

$$\Delta w+k_w^2w=0, \quad z<g(x), \tag{3.3}$$

subject to the Dirichlet condition, $w(x,g(x))=W(x)$, the Neumann data, $\tilde{W}(x)$, can be computed. The DNO J is defined by

$$J(g):W\to\tilde{W}.$$

Negating the second equation, (3.1) can now be written as

$$\begin{pmatrix} I & -I+A\tau_wJ \\ \tau_uG & \tau_wJ-B \end{pmatrix}\begin{pmatrix} U \\ W \end{pmatrix}=\begin{pmatrix} \xi \\ -\tau_u\nu \end{pmatrix}. \tag{3.4}$$

3.1 The patterned, flat–interface configuration

The configurations of interest to engineers [2,15] often feature *flat* layer interfaces with *patterned* graphene sandwiched in between. For this we use the modeling assumptions

$$g(x)\equiv 0, \quad \hat{\sigma}\approx\hat{\sigma}_{\text{BGK}}X(x;\delta),$$

where $\hat{\sigma}_{\text{BGK}}$ is a (dimensionless) Bhatnagar–Gross–Krook (BGK) model for the graphene [8],

$$\hat{\sigma}_{\text{BGK}}=\hat{\sigma}_{\text{Drude}}\left\{1-v_F^2\left(\frac{3f+2i/\tau}{4f(f+i/\tau)^2}\right)\partial_x^2\right\}=:\hat{\sigma}_{\text{loc}}-\hat{\sigma}_{\text{nloc}}\partial_x^2,$$

where the local term comes from a Drude model [2,15],

$$\hat{\sigma}_{\text{Drude}}=\frac{\sigma_0}{\epsilon_0c_0}\left(\frac{4E_F}{\pi}\right)\frac{1}{\hbar\tilde{\gamma}-i\hbar\omega}=\frac{2E_Fe^2}{\epsilon_0c_0}\left(\frac{1}{\Gamma-ihf}\right),$$

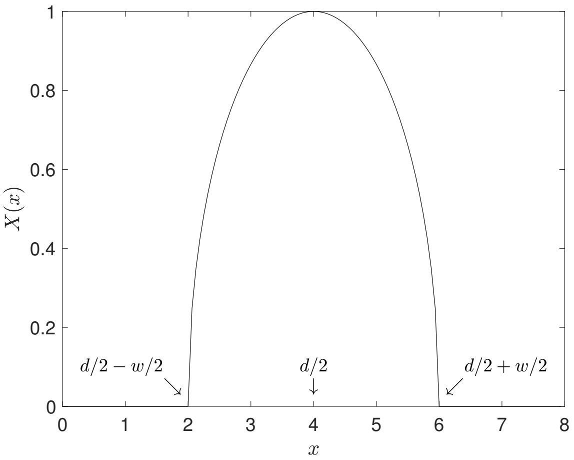

Figure 2: Plot of the current envelope function, $X(x)=X_0+X_1(x)$.

where $\sigma_0=\pi e^2/(2h)$ is the universal AC conductivity of graphene [15], $e>0$ is the elementary charge, h is Planck's constant, $\hbar=h/(2\pi)$, E_F is the (local) Fermi level position, and $\tilde{\gamma}$ is the relaxation rate. ($\Gamma=\hbar\tilde{\gamma}$ is another frequently used notation.) Further, v_F is the Fermi velocity, $f=\omega/(2\pi)$ is the ordinary frequency of the incident radiation, and τ is the carrier lifetime. We will also have use for the following decomposition of $A=A_{\text{loc}}-A_{\text{nloc}}$ and $B=B_{\text{loc}}-B_{\text{nloc}}$,

$$A_{\text{loc}}=\begin{cases}0, & \text{TE},\\ |N|\hat{\sigma}_{\text{loc}}/(ik_0), & \text{TM},\end{cases}\qquad A_{\text{nloc}}=\begin{cases}0, & \text{TE},\\ |N|(\hat{\sigma}_{\text{nloc}}/(ik_0))\partial_x^2, & \text{TM},\end{cases}$$

and

$$B_{\text{loc}}=\begin{cases}(ik_0)\hat{\sigma}_{\text{loc}}/|N|, & \text{TE},\\ 0, & \text{TM},\end{cases}\qquad B_{\text{nloc}}=\begin{cases}(ik_0)(\hat{\sigma}_{\text{nloc}}/|N|)\partial_x^2, & \text{TE},\\ 0, & \text{TM}.\end{cases}$$

Also, $X(x;\delta)$ is a d–periodic (in x) *envelope* function which we use to model the patterning. For this we permit the envelope to be varied with a parameter δ, e.g.,

$$X(x;\delta)=X_0+\delta X_1(x), \tag{3.5}$$

where $X_0\neq 0$ as explained below, and

$$X_1(x)=-X_0+\begin{cases}\sqrt{1-4\left(\frac{x-d/2}{w}\right)^2}, & d/2-w/2<x<d/2+w/2,\\ 0, & \text{else},\end{cases} \tag{3.6}$$

and w is the ribbon width; see Fig. 2. This profile was specified in [2] to model not only the patterning but also edge effects.

With these assumptions, and denoting $G_0 = G(0)$ and $J_0 = J(0)$, we consider the modification of (3.4),

$$\begin{pmatrix} I & -I + AX(x;\delta)\tau_w J_0 \\ \tau_u G_0 & \tau_w J_0 - BX(x;\delta) \end{pmatrix} \begin{pmatrix} U \\ W \end{pmatrix} = \begin{pmatrix} \xi \\ -\tau_u \nu \end{pmatrix}. \tag{3.7}$$

Remark 3.1. Importantly, in the flat–interface case, $g(x) \equiv 0$, the DNOs can be explicitly specified in terms of Fourier multipliers. Considering the upper layer DNO, G_0, we recall the Rayleigh expansions [38,44]

$$u(x,z) = \sum_{p=-\infty}^{\infty} \hat{U}_p e^{i\alpha_p x + i\gamma_{u,p} z}, \tag{3.8}$$

where

$$\alpha_p = \alpha + (2\pi/d)p, \quad \gamma_{m,p} = \begin{cases} \sqrt{k_m^2 - \alpha_p^2}, & p \in \mathcal{U}_m, \\ i\sqrt{\alpha_p^2 - k_m^2}, & p \notin \mathcal{U}_m, \end{cases} \quad m \in \{u,w\}, \tag{3.9a}$$

and the propagating modes are

$$\mathcal{U}_m := \left\{ p \in \mathbf{Z} \mid \alpha_p^2 \le k_m^2 \right\}, \quad m \in \{u,w\}, \tag{3.9b}$$

which gives the exact solution of (3.2) with Dirichlet data $u(x,0) = U(x)$. From this the Neumann data can readily be shown to be

$$\tilde{U}(x) = -\partial_z u(x,0) = \sum_{p=-\infty}^{\infty} -i\gamma_{u,p} \hat{U}_p e^{i\alpha_p x},$$

which gives

$$G_0[U] = \sum_{p=-\infty}^{\infty} -i\gamma_{u,p} \hat{U}_p e^{i\alpha_p x} =: -i\gamma_{u,D} U,$$

defining the order–one Fourier multiplier, $\gamma_{u,D}$. In analogous fashion, based on the Rayleigh expansion solution of (3.3),

$$w(x,z) = \sum_{p=-\infty}^{\infty} \hat{W}_p e^{i\alpha_p x - i\gamma_{w,p} z}, \tag{3.10}$$

one can demonstrate that

$$J_0[W] = \sum_{p=-\infty}^{\infty} -i\gamma_{w,p} \hat{W}_p e^{i\alpha_p x} =: -i\gamma_{w,D} W.$$

3.2 A high–order perturbation of envelopes method

As we shall see, (3.7) is straightforward to solve provided that $X(x) \equiv X_0 \in \mathbf{R}$. In this case the equations are diagonalized by the Fourier transform and the solution can be found wavenumber–by–wavenumber. We build upon this observation by considering envelope functions of the form (3.5) and proceeding with (regular) perturbation theory. As we are considering deformations of the envelope (through the parameter δ), we term such a scheme a "High–Order Perturbation of Envelopes" (HOPE) method to contrast with "High–Order Perturbation of Surfaces" (HOPS) algorithms where the height/slope of the interface *shape* is the perturbation parameter [33].

For this HOPE approach we posit expansions

$$\{U,W\} = \{U,W\}(x;\delta) = \sum_{\ell=0}^{\infty} \{U_\ell, W_\ell\}(x)\delta^\ell, \tag{3.11}$$

and derive recursive formulas for the $\{U_\ell, W_\ell\}$. It is not difficult to see that, at order $\ell \geq 0$, one must solve

$$\begin{pmatrix} I & -I + AX_0\tau_w J_0 \\ \tau_u G_0 & \tau_w J_0 - BX_0 \end{pmatrix} \begin{pmatrix} U_\ell \\ W_\ell \end{pmatrix} = \delta_{\ell,0} \begin{pmatrix} \xi \\ -\tau_u \nu \end{pmatrix} + \begin{pmatrix} -AX_1(x)\tau_w J_0 W_{\ell-1} \\ BX_1(x) W_{\ell-1} \end{pmatrix}, \tag{3.12}$$

where $\delta_{\ell,q}$ is the Kronecker delta, and $W_{-1} \equiv 0$. We will presently show that (3.11) converge strongly in appropriate Sobolev spaces. Importantly, these recursions also result in a numerical algorithm that delivers HOS accuracy.

Remark 3.2. As we have pointed out that the operators G_0 and J_0 are diagonalized by the Fourier transform, we can state the condition of "non–resonance" which we require for uniqueness of solutions. As we shall see, in Transverse Electric (TE) polarization ($A = 0$ and $\tau_m = 1$) we will require that the determinant function

$$\begin{aligned} \Delta_p^{\mathrm{TE}} &:= \widehat{(G_0)}_p + \widehat{(J_0)}_p - BX_0 \\ &= -i\gamma_{u,p} - i\gamma_{w,p} - ik_0\hat{\sigma}_{\mathrm{loc}} X_0 - ik_0 \hat{\sigma}_{\mathrm{nloc}} X_0 \alpha_p^2, \end{aligned} \tag{3.13}$$

satisfies, for some $\mu > 0$, $\min_{-\infty<p<\infty} \left\{ \left| \Delta_p^{\mathrm{TE}} \right| \right\} > \mu$. In Transverse Magnetic (TM) polarization ($B = 0$) it must be that the determinant function

$$\begin{aligned} \Delta_p^{\mathrm{TM}} &:= \tau_u \widehat{(G_0)}_p + \tau_w \widehat{(J_0)}_p - \tau_u \tau_w A X_0 \widehat{(G_0)}_p \widehat{(J_0)}_p \\ &= -\tau_u i\gamma_{u,p} - \tau_w i \gamma_{w,p} + \tau_u \tau_w \left(\frac{\hat{\sigma}_{\mathrm{loc}}}{ik_0} \right) X_0 \gamma_{u,p} \gamma_{w,p} \\ &\quad + \tau_u \tau_w \left(\frac{\hat{\sigma}_{\mathrm{nloc}}}{ik_0} \right) X_0 \gamma_{u,p} \gamma_{w,p} \alpha_p^2, \end{aligned} \tag{3.14}$$

satisfies, for some $\mu > 0$, $\min_{-\infty<p<\infty} \left\{ \left| \Delta_p^{\mathrm{TM}} \right| \right\} > \mu$.

We now describe precise progress on this in the following lemma.

Lemma 3.1. *If* $X_0>0$*, for any* $p\in\mathbf{Z}$

$$\Delta_p^{TE}\neq 0,\quad \Delta_p^{TM}\neq 0.$$

Proof. We begin with the notation

$$z=z'+iz''\in\mathbf{C},\quad z',z''\in\mathbf{R},$$

and recall that, for $\hat{\sigma}_{\text{loc}}=\hat{\sigma}'_{\text{loc}}+i\hat{\sigma}''_{\text{loc}}$,

$$\hat{\sigma}'_{\text{loc}}=\frac{(2E_Fe^2)\Gamma}{\epsilon_0c_0(\Gamma^2+h^2f^2)}>0,\quad \hat{\sigma}''_{\text{loc}}=\frac{(2E_Fe^2)hf}{\epsilon_0c_0(\Gamma^2+h^2f^2)}>0.$$

Furthermore, we have, c.f. (3.9),

$$\gamma_{m,p}=\begin{cases}\gamma'_{m,p}, & p\in\mathcal{U}_m,\\ i\gamma''_{m,p}, & p\notin\mathcal{U}_m,\end{cases}\quad \gamma'_{m,p},\gamma''_{m,p}\geq 0,$$

for $m\in\{u,w\}$, so that either

$$\{\gamma'_{m,p}\geq 0 \text{ and } \gamma''_{m,p}=0\}\quad\text{or}\quad\{\gamma'_{m,p}=0 \text{ and } \gamma''_{m,p}\geq 0\}.$$

From the nonlocal current model we examine the term

$$Q=v_F^2\left(\frac{3f+2i/\tau}{4f(f+i/\tau)^2}\right),$$

and calculate

$$\begin{aligned}Q&=\frac{v_F^2\tau(3f\tau+2i)}{4f(f\tau+i)^2}=\frac{v_F^2\tau}{4f(f^2\tau^2+1)^2}(3f\tau+2i)(f\tau-i)^2\\&=\frac{v_F^2\tau}{4f(f^2\tau^2+1)^2}[f\tau(3f^2\tau^2+1)-2i(2f^2\tau^2+1)],\end{aligned}$$

therefore we have

$$Q'=\frac{v_F^2\tau^2(3f^2\tau^2+1)}{4(f^2\tau^2+1)^2}>0,\quad Q''=-\frac{v_F^2\tau(2f^2\tau^2+1)}{2f(f^2\tau^2+1)^2}<0.$$

Finally, another crucial term in both polarizations is

$$\begin{aligned}\Sigma&:=\hat{\sigma}_{\text{loc}}\left(1+Q\alpha_p^2\right)\\&=\left(\hat{\sigma}'_{\text{loc}}+i\hat{\sigma}''_{\text{loc}}\right)\left((1+Q'\alpha_p^2)+iQ''\alpha_p^2\right)\\&=\left(\hat{\sigma}'_{\text{loc}}(1+Q'\alpha_p^2)-\hat{\sigma}''_{\text{loc}}Q''\alpha_p^2\right)+i\left(\hat{\sigma}'_{\text{loc}}Q''\alpha_p^2+\hat{\sigma}''_{\text{loc}}(1+Q'\alpha_p^2)\right).\end{aligned}$$

While the imaginary part is indeterminate, we can state that, due to the signs of $\{\hat{\sigma}'_{\mathrm{loc}},\hat{\sigma}''_{\mathrm{loc}},Q',Q''\}$, the real part satisfies

$$\Sigma' = \mathrm{Re}\{\Sigma\} = \hat{\sigma}'_{\mathrm{loc}}(1+Q'\alpha^2) - \hat{\sigma}''_{\mathrm{loc}}Q''\alpha_p^2 > 0.$$

We begin with the case of TE polarization where we have, from the parity of Σ',

$$\mathrm{Re}\{i\Delta_p^{\mathrm{TE}}\} = \gamma'_{u,p} + \gamma'_{w,p} + k_0 X_0 \Sigma' > 0.$$

For TM polarization we have

$$i\Delta_p^{\mathrm{TM}} = \tau_u\gamma_{u,p} + \tau_w\gamma_{w,p} + \tau_u\gamma_{u,p}\tau_w\gamma_{w,p}\left(\frac{X_0}{k_0}\right)\Sigma,$$

and begin with the case of a Rayleigh singularity in the upper layer, $\gamma_{u,p}=0$. We point out that, if $\epsilon_w \neq \epsilon_u$ then $\gamma_{w,p} \neq \gamma_{u,p} = 0$ for this choice of p. In this case

$$i\Delta_p^{\mathrm{TM}} = \tau_w\gamma_{w,p} \neq 0.$$

Clearly, a Rayleigh singularity in the lower layer, $\gamma_{w,p}=0$, can be handled similarly. So, we now fix on the situation of no Rayleigh singularities,

$$\{\gamma'_{m,p} > 0 \text{ and } \gamma''_{m,p} = 0\} \quad \text{or} \quad \{\gamma'_{m,p} = 0 \text{ and } \gamma''_{m,p} > 0\},$$

and divide the calculation into four parts:

1. Case $\gamma'_{u,p} = \gamma'_{w,p} = 0$. Here
$$\mathrm{Re}\{i\Delta_p^{\mathrm{TM}}\} = -\tau_u\gamma''_{u,p}\tau_w\gamma''_{w,p}\left(\frac{X_0}{k_0}\right)\Sigma' < 0.$$
2. Case $\gamma'_{u,p} = \gamma''_{w,p} = 0$. Here
$$\mathrm{Im}\{i\Delta_p^{\mathrm{TM}}\} = \tau_u\gamma''_{u,p} + \tau_u\gamma''_{u,p}\tau_w\gamma'_{w,p}\left(\frac{X_0}{k_0}\right)\Sigma' > 0.$$
3. Case $\gamma''_{u,p} = \gamma'_{w,p} = 0$. Here
$$\mathrm{Im}\{i\Delta_p^{\mathrm{TM}}\} = \tau_w\gamma''_{w,p} + \tau_u\gamma'_{u,p}\tau_w\gamma''_{w,p}\left(\frac{X_0}{k_0}\right)\Sigma' > 0.$$
4. Case $\gamma''_{u,p} = \gamma''_{w,p} = 0$. Here
$$\mathrm{Re}\{i\Delta_p^{\mathrm{TM}}\} = \tau_u\gamma'_{u,p} + \tau_w\gamma'_{w,p} + \tau_u\gamma'_{u,p}\tau_w\gamma'_{w,p}\left(\frac{X_0}{k_0}\right)\Sigma' > 0.$$

The conclusion of these four computations is that $\Delta_p^{\mathrm{TM}} \neq 0$. □

4 Analyticity

Before describing our theoretical results we pause to specify the function spaces we will require. For any real $s \geq 0$ we recall the classical L^2–based Sobolev norm

$$\|U\|_{H^s}^2 := \sum_{p=-\infty}^{\infty} \langle p \rangle^{2s} \left| \hat{U}_p \right|^2, \quad \langle p \rangle^2 := 1 + |p|^2, \quad \hat{U}_p := \frac{1}{d} \int_0^d U(x) e^{i\alpha_p x} \, dx,$$

which gives rise to the Sobolev space

$$H^s([0,d]) := \left\{ U(x) \in L^2([0,d]) \mid \|U\|_{H^s} < \infty \right\}.$$

With this definition it is a simple matter to prove the following lemma.

Lemma 4.1. *For any real $s \geq 0$ there exist constants $C_G, C_J > 0$ such that*

$$\|G_0 U\|_{H^s} \leq C_G \|U\|_{H^{s+1}}, \quad \|J_0 W\|_{H^s} \leq C_J \|W\|_{H^{s+1}},$$

for any $U, W \in H^{s+1}$.

We also recall, for any integer $s \geq 0$, the space of s–times continuously differentiable functions with the Hölder norm

$$|f|_{C^s} = \max_{0 \leq \ell \leq s} \left| \partial_x^\ell f \right|_{L^\infty}.$$

For later reference we recall the classical result [7].

Lemma 4.2. *For any integer $s \geq 0$ there exists a constant $K = K(s)$ such that*

$$\|fU\|_{H^s} \leq K |f|_{C^s} \|U\|_{H^s}.$$

We now begin the rigorous analysis of the expansions (3.11) and, for this, we appeal to the general theory of analyticity of solutions of linear systems of equations. For a particular description of the procedure, we follow the developments found in [28] for the solution of

$$\mathbf{A}(\delta)\mathbf{V}(\delta) = \mathbf{R}(\delta), \tag{4.1}$$

which is (3.1) of [28] with ε replaced by δ. In [28], given expansions

$$\mathbf{A}(\delta) = \sum_{\ell=0}^{\infty} \mathbf{A}_\ell \delta^\ell, \quad \mathbf{R}(\delta) = \sum_{\ell=0}^{\infty} \mathbf{R}_\ell \delta^\ell, \tag{4.2}$$

we seek a solution of the form

$$\mathbf{V}(\delta) = \sum_{\ell=0}^{\infty} \mathbf{V}_\ell \delta^\ell, \tag{4.3}$$

which satisfies

$$\mathbf{V}_\ell = \mathbf{A}_0^{-1} \left[\mathbf{R}_\ell - \sum_{q=0}^{\ell-1} \mathbf{A}_{\ell-q} \mathbf{V}_q \right], \quad \ell \geq 0.$$

We restate the main result here for completeness.

Theorem 4.1 ([28]). *Given two Banach spaces Y and Z, suppose that:*

(H1) $\mathbf{R}_\ell \in Z$ *for all* $\ell \geq 0$, *and there exist constants* $C_R > 0$, $B_R > 0$ *such that*

$$\|\mathbf{R}_\ell\|_Y \leq C_R B_R^\ell, \quad \ell \geq 0.$$

(H2) $\mathbf{A}_\ell : Y \to Z$ *for all* $\ell \geq 0$, *and there exists constants* $C_A > 0$, $B_A > 0$ *such that*

$$\|\mathbf{A}_\ell\|_{Y\to Z} \leq C_A B_A^\ell, \quad \ell \geq 0.$$

(H3) $\mathbf{A}_0^{-1} : Z \to Y$, *and there exists a constant* $C_e > 0$ *such that*

$$\left\|\mathbf{A}_0^{-1}\right\|_{Z\to Y} \leq C_e.$$

Then the equation (4.1) *has a unique solution* (4.3), *and there exist constants* $C_V > 0$ *and* $B_V > 0$ *such that*

$$\|\mathbf{V}_\ell\|_Y \leq C_V B_V^\ell, \quad \ell \geq 0,$$

for any

$$C_V \geq 2C_e C_R, \quad B_V \geq \max\{B_R, 2B_A, 4C_e C_A B_A\},$$

which implies that, for any $0 \leq \rho < 1$, (4.3) *converges for all* δ *such that* $B_V \delta < \rho$, *i.e.,* $\delta < \rho / B_V$.

From (3.7) it is easy to identify

$$\mathbf{A} = \begin{pmatrix} I & -I + AX(x;\delta)\tau_w J_0 \\ \tau_u G_0 & \tau_w J_0 - BX(x;\delta) \end{pmatrix}, \quad \mathbf{V} = \begin{pmatrix} U \\ W \end{pmatrix}, \quad \mathbf{R} = \begin{pmatrix} \xi \\ -\tau_u \nu \end{pmatrix}.$$

All that remains is to find the forms (4.2), and establish Hypotheses (H1), (H2), and (H3). As we shall shortly see, the analysis depends strongly upon the polarization (TE/TM) of our fields so we break our developments into these two cases.

4.1 Transverse electric polarization

In Transverse Electric polarization $A \equiv 0$ and $\tau_m = 1$, and we see that (3.7) becomes

$$\begin{pmatrix} I & -I \\ G_0 & J_0 - BX(x;\delta) \end{pmatrix} \begin{pmatrix} U \\ W \end{pmatrix} = \begin{pmatrix} \xi \\ -\nu \end{pmatrix}, \tag{4.4}$$

so that

$$\mathbf{A}_0 = \begin{pmatrix} I & -I \\ G_0 & J_0 - BX_0 \end{pmatrix}; \quad \mathbf{A}_1 = \begin{pmatrix} 0 & 0 \\ 0 & -BX_1(x) \end{pmatrix}; \quad \mathbf{A}_\ell \equiv \begin{pmatrix} 0 & 0 \\ 0 & 0 \end{pmatrix}, \quad \ell \geq 2,$$

and

$$\mathbf{R}_0 = \begin{pmatrix} \xi \\ -\nu \end{pmatrix}; \quad \mathbf{R}_\ell \equiv \begin{pmatrix} 0 \\ 0 \end{pmatrix}, \quad \ell \geq 1.$$

As we shall see in the next Lemma, the natural spaces in which to work for TE polarization are, for real $s \geq 0$,

$$Y = H^{s+1} \times H^{s+2}, \quad Z = H^{s+1} \times H^{s},$$

so that

$$\left\| \underline{y} \right\|_Y^2 = \left\| \underline{y}_1 \right\|_{H^{s+1}}^2 + \left\| \underline{y}_2 \right\|_{H^{s+2}}^2, \quad \|\underline{z}\|_Z^2 = \|\underline{z}_1\|_{H^{s+1}}^2 + \|\underline{z}_2\|_{H^s}^2.$$

Hypothesis (H1): With these definitions it is a simple matter to show that

$$\|\mathbf{R}_0\|_Z^2 = \|\xi\|_{H^{s+1}}^2 + \|\nu\|_{H^s}^2 < \infty,$$

given that

$$\xi = -e^{i\alpha x}, \quad \nu = i\gamma_u e^{i\alpha x},$$

so that $\xi, \nu \in H^t$ for any real $t \geq 0$. Thus Hypothesis (H1) is established with any choices of C_R and B_R such that $C_R B_R = \|\mathbf{R}_0\|_Z$.

Hypothesis (H2): Considering generic $U \in H^{s+1}$ and $W \in H^{s+2}$ we study

$$\begin{aligned}
\left\| \mathbf{A}_0 \begin{pmatrix} U \\ W \end{pmatrix} \right\|_Z^2 &= \|U - W\|_{H^{s+1}}^2 + \|G_0 U + J_0 W - B X_0 W\|_{H^s}^2 \\
&\leq \|U\|_{H^{s+1}}^2 + \|W\|_{H^{s+1}}^2 + C_G^2 \|U\|_{H^{s+1}}^2 + C_J^2 \|W\|_{H^{s+1}}^2 \\
&\quad + |ik_0 \hat{\sigma}_{\text{loc}}|^2 |X_0|^2 \|W\|_{H^s}^2 + |ik_0 \hat{\sigma}_{\text{nloc}}|^2 |X_0|^2 \left\|\partial_x^2 W\right\|_{H^s}^2 \\
&\leq C_0^2 \left(\|U\|_{H^{s+1}}^2 + \|W\|_{H^{s+2}}^2 \right) \\
&= C_0^2 \left\| \begin{pmatrix} U \\ W \end{pmatrix} \right\|_Y^2,
\end{aligned}$$

where we have used Lemma 4.1, and we have the desired mapping property of $\mathbf{A}_0$. We turn to $\mathbf{A}_1$ and find

$$\begin{aligned}
\left\| \mathbf{A}_1 \begin{pmatrix} U \\ W \end{pmatrix} \right\|_Z^2 &= \|-B X_1(x) W\|_{H^s}^2 \\
&\leq |ik_0 \hat{\sigma}_{\text{loc}}|^2 K^2 |X_1|_{C^s}^2 \|W\|_{H^s}^2 + |ik_0 \hat{\sigma}_{\text{nloc}}|^2 K^2 |X_1|_{C^s}^2 \left\|\partial_x^2 W\right\|_{H^s}^2 \\
&\leq C_1^2 |X_1|_{C^s}^2 \|W\|_{H^{s+2}}^2 \\
&\leq C_1^2 |X_1|_{C^s}^2 \left\| \begin{pmatrix} U \\ W \end{pmatrix} \right\|_Y^2,
\end{aligned}$$

where we have used the Algebra property, Lemma 4.2, which mandates integer $s \geq 0$. Thus, we are done with Hypothesis (H2) if we choose $C_A = \max\{C_0, C_1\}$ and $B_A = |X_1|_{C^s}$.

Hypothesis (H3): The crux of the matter, as always in regular perturbation theory, is the invertibility of the linearized operator $\mathbf{A}_0$ and its mapping properties. For this we prove the following result.

Lemma 4.3. *Given real* $s\geq 0$ *if* $Q\in H^{s+1}$ *and* $R\in H^s$, *and* $X_0\neq 0$ *then there exists a unique solution of*

$$\begin{pmatrix} I & -I \\ G_0 & J_0-BX_0 \end{pmatrix}\begin{pmatrix} U \\ W \end{pmatrix}=\begin{pmatrix} Q \\ R \end{pmatrix}, \tag{4.5}$$

satisfying

$$\|U\|_{H^{s+1}}\leq C_e\{\|Q\|_{H^{s+1}}+\|R\|_{H^s}\},$$
$$\|W\|_{H^{s+2}}\leq C_e\{\|Q\|_{H^{s+1}}+\|R\|_{H^s}\},$$

for some constant $C_e>0$.

Proof. Upon expressing

$$U(x)=\sum_{p=-\infty}^{\infty}\hat{U}_p e^{i\alpha_p x},\quad W(x)=\sum_{p=-\infty}^{\infty}\hat{W}_p e^{i\alpha_p x},$$

we find that (4.5) demands

$$\begin{pmatrix} 1 & -1 \\ -i\gamma_{u,p} & -i\gamma_{w,p}-B_{\text{loc}}X_0+B_{\text{nloc}}X_0 \end{pmatrix}\begin{pmatrix} \hat{U}_p \\ \hat{W}_p \end{pmatrix}=\begin{pmatrix} \hat{Q}_p \\ \hat{R}_p \end{pmatrix}.$$

The exact solution is easily seen to be

$$\hat{U}_p=\frac{\{i\gamma_{w,p}+(ik_0)\hat{\sigma}_{\text{loc}}X_0+(ik_0)\hat{\sigma}_{\text{nloc}}X_0\alpha_p^2\}\hat{Q}_p+\hat{R}_p}{\Delta_p^{\text{TE}}},$$
$$\hat{W}_p=\frac{i\gamma_{u,p}\hat{Q}_p+\hat{R}_p}{\Delta_p^{\text{TE}}}.$$

Since we are "nonresonant" (see Remark 3.2) and, since $X_0\neq 0$, $1/\Delta_p^{\text{TE}}=\mathcal{O}(\langle p\rangle^{-2})$ as $p\to\infty$ we find

$$\|U\|_{H^{s+1}}^2=\sum_{p=-\infty}^{\infty}\langle p\rangle^{2(s+1)}\left|\hat{U}_p\right|^2\leq\sum_{p=-\infty}^{\infty}\langle p\rangle^{2(s+1)}\left\{C_Q\left|\hat{Q}_p\right|^2+C_R\langle p\rangle^{-4}\left|\hat{R}_p\right|^2\right\},$$

which delivers

$$\|U\|_{H^{s+1}}\leq C_e\{\|Q\|_{H^{s+1}}+\|R\|_{H^{s-1}}\}\leq C_e\{\|Q\|_{H^{s+1}}+\|R\|_{H^s}\}.$$

In a similar manner,

$$\|W\|_{H^{s+2}}^2=\sum_{p=-\infty}^{\infty}\langle p\rangle^{2(s+2)}\left|\hat{W}_p\right|^2\leq\sum_{p=-\infty}^{\infty}\langle p\rangle^{2(s+2)}\left\{\langle p\rangle^{-2}C_Q\left|\hat{Q}_p\right|^2+C_R\langle p\rangle^{-4}\left|\hat{R}_p\right|^2\right\},$$

which gives

$$\|W\|_{H^{s+2}}\leq C_e\{\|Q\|_{H^{s+1}}+\|R\|_{H^s}\}.$$

This completes the proof. □

Having established Hypotheses (H1), (H2), and (H3) we can invoke Theorem 4.1 to deduce.

Theorem 4.2. *Given an integer* $s \geq 0$*, if* $X_0 \neq 0$ *and* $X_1 \in C^s([0,d])$ *there exists a unique solution pair,* (3.11)*, of the TE problem* (4.4) *satisfying*

$$\|U_\ell\|_{H^{s+1}} \leq C_U D^\ell, \quad \|W_\ell\|_{H^{s+2}} \leq C_W D^\ell, \quad \forall\, \ell \geq 0, \tag{4.6}$$

for any $D > C|X_1|_{C^s}$ *where* C_U *and* C_W *are constants.*

4.2 Transverse magnetic polarization

Meanwhile, in Transverse Magnetic polarization $B \equiv 0$ and we see that (3.7) becomes

$$\begin{pmatrix} I & -I + AX\tau_w J_0 \\ \tau_u G_0 & \tau_w J_0 \end{pmatrix} \begin{pmatrix} U \\ W \end{pmatrix} = \begin{pmatrix} \xi \\ -\tau_u \nu \end{pmatrix}, \tag{4.7}$$

so that

$$\mathbf{A}_0 = \begin{pmatrix} I & -I + AX_0\tau_w J_0 \\ \tau_u G_0 & \tau_w J_0 \end{pmatrix}; \quad \mathbf{A}_1 = \begin{pmatrix} 0 & AX_1(x)\tau_w J_0 \\ 0 & 0 \end{pmatrix}; \quad \mathbf{A}_\ell \equiv \begin{pmatrix} 0 & 0 \\ 0 & 0 \end{pmatrix}, \quad \ell \geq 2,$$

and,

$$\mathbf{R}_0 = \begin{pmatrix} \xi \\ -\tau_u \nu \end{pmatrix}; \quad \mathbf{R}_\ell \equiv \begin{pmatrix} 0 \\ 0 \end{pmatrix}, \quad \ell \geq 1.$$

It will become clear presently that the natural spaces for TM polarization are, for real $s \geq 0$,

$$Y = H^{s+1} \times H^{s+3}, \quad Z = H^s \times H^s,$$

so that

$$\left\|\underline{y}\right\|_Y^2 = \left\|\underline{y}_1\right\|_{H^{s+1}}^2 + \left\|\underline{y}_2\right\|_{H^{s+3}}^2, \quad \|\underline{z}\|_Z^2 = \|\underline{z}_1\|_{H^s}^2 + \|\underline{z}_2\|_{H^s}^2.$$

Hypothesis (H1): Akin to the TE case

$$\|\mathbf{R}_0\|_Z^2 = \|\xi\|_{H^s}^2 + \|\tau_u \nu\|_{H^s}^2 < \infty,$$

and Hypothesis (H1) is established with any choices of C_R and B_R such that $C_R B_R = \|\mathbf{R}_0\|_Z$.

Hypothesis (H2): Once again, considering generic $U\in H^{s+1}$ and $W\in H^{s+3}$ we consider

$$\begin{aligned}\left\|\mathbf{A}_0\begin{pmatrix}U\\W\end{pmatrix}\right\|_Z^2&=\|U-W+AX_0\tau_w J_0 W\|_{H^s}^2+\|\tau_u G_0 U+\tau_w J_0 W\|_{H^s}^2\\&\le\|U\|_{H^s}^2+\|W\|_{H^s}^2+|\tau_u|^2 C_G^2\|U\|_{H^{s+1}}^2\\&\quad+\left\{\left|\frac{\hat{\sigma}_{\text{loc}}}{ik_0}\right|^2|X_0|^2+1\right\}|\tau_w|^2 C_J^2\|W\|_{H^{s+1}}^2+\left\{\left|\frac{\hat{\sigma}_{\text{nloc}}}{ik_0}\right|^2|X_0|^2\right\}|\tau_w|^2 C_J^2\left\|\partial_x^2 W\right\|_{H^{s+1}}^2\\&\le C_0^2\left(\|U\|_{H^{s+1}}^2+\|W\|_{H^{s+3}}^2\right)\\&=C_0^2\left\|\begin{pmatrix}U\\W\end{pmatrix}\right\|_Y^2,\end{aligned}$$

again using Lemma 4.1, and we have the required mapping property of $\mathbf{A}_0$. We now consider $\mathbf{A}_1$

$$\begin{aligned}\left\|\mathbf{A}_1\begin{pmatrix}U\\W\end{pmatrix}\right\|_Z^2&=\|AX_1(x)\tau_w J_0 W\|_{H^s}^2\\&\le\left|\frac{\hat{\sigma}_{\text{loc}}}{ik_0}\right|^2 K^2|X_1|_{C^s}^2|\tau_w|^2\|W\|_{H^{s+1}}^2+\left|\frac{\hat{\sigma}_{\text{nloc}}}{ik_0}\right|^2 K^2|X_1|_{C^s}^2|\tau_w|^2\left\|\partial_x^2 W\right\|_{H^{s+1}}^2\\&\le C_1^2|X_1|_{C^s}^2\|W\|_{H^{s+3}}^2\\&\le C_1^2|X_1|_{C^s}^2\left\|\begin{pmatrix}U\\W\end{pmatrix}\right\|_Y^2,\end{aligned}$$

where we have used Lemma 4.2. Thus, we are done with Hypothesis (H2) if we choose $C_A=\max\{C_0,C_1\}$ and $B_A=|X_1|_{C^s}$.

Hypothesis (H3): We now study the invertibility of the operator $\mathbf{A}_0$.

Lemma 4.4. *Given real $s\ge 0$ if $Q\in H^s$, $R\in H^s$, and $X_0\neq 0$ then there exists a unique solution of*

$$\begin{pmatrix}I&-I+AX_0\tau_w J_0\\\tau_u G_0&\tau_w J_0\end{pmatrix}\begin{pmatrix}U\\W\end{pmatrix}=\begin{pmatrix}Q\\R\end{pmatrix},\tag{4.8}$$

satisfying

$$\begin{aligned}\|U\|_{H^{s+1}}&\le C_e\{\|Q\|_{H^s}+\|R\|_{H^s}\},\\\|W\|_{H^{s+3}}&\le C_e\{\|Q\|_{H^s}+\|R\|_{H^s}\},\end{aligned}$$

for some constant $C_e>0$.

Proof. With

$$U(x)=\sum_{p=-\infty}^{\infty}\hat{U}_p e^{i\alpha_p x},\quad W(x)=\sum_{p=-\infty}^{\infty}\hat{W}_p e^{i\alpha_p x},$$

we find that (4.8) requires

$$\begin{pmatrix} 1 & -1-AX_0\tau_w i\gamma_{w,p} \\ -\tau_u i\gamma_{u,p} & -\tau_w i\gamma_{w,p} \end{pmatrix} \begin{pmatrix} \hat{U}_p \\ \hat{W}_p \end{pmatrix} = \begin{pmatrix} \hat{Q}_p \\ \hat{R}_p \end{pmatrix}.$$

The exact solution is easily seen to be

$$\hat{U}_p = \frac{-\tau_w i\gamma_{w,p}\hat{Q}_p + \left\{1+\frac{X_0}{ik_0}(\hat{\sigma}_{\mathrm{loc}}+\hat{\sigma}_{\mathrm{nloc}}\alpha_p^2)\right\}\tau_w i\gamma_{w,p}\hat{R}_p}{\Delta_p^{\mathrm{TM}}},$$

$$\hat{W}_p = \frac{\tau_u i\gamma_{u,p}\hat{Q}_p + \hat{R}_p}{\Delta_p^{\mathrm{TM}}}.$$

Once again, as we are “nonresonant” (Remark 3.2) and, since $X_0 \neq 0$, $1/\Delta_p^{\mathrm{TM}} = \mathcal{O}(\langle p\rangle^{-4})$ as $p\to\infty$ we find

$$\|U\|_{H^{s+1}}^2 = \sum_{p=-\infty}^{\infty} \langle p\rangle^{2(s+1)} |\hat{U}_p|^2 \leq \sum_{p=-\infty}^{\infty} \langle p\rangle^{2(s+1)} \left\{C_Q\langle p\rangle^{-6}|\hat{Q}_p|^2 + C_R\langle p\rangle^{-2}|\hat{R}_p|^2\right\},$$

which gives

$$\|U\|_{H^{s+1}} \leq C_e\{\|Q\|_{H^{s-2}}+\|R\|_{H^s}\} \leq C_e\{\|Q\|_{H^s}+\|R\|_{H^s}\}.$$

Similarly,

$$\|W\|_{H^{s+3}}^2 = \sum_{p=-\infty}^{\infty} \langle p\rangle^{2(s+3)} |\hat{W}_p|^2 \leq \sum_{p=-\infty}^{\infty} \langle p\rangle^{2(s+3)} \left\{C_Q\langle p\rangle^{-6}|\hat{Q}_p|^2 + C_R\langle p\rangle^{-8}|\hat{R}_p|^2\right\},$$

which delivers

$$\|W\|_{H^{s+3}} \leq C_e\{\|Q\|_{H^s}+\|R\|_{H^{s-1}}\} \leq C_e\{\|Q\|_{H^s}+\|R\|_{H^s}\}.$$

This completes the proof. □

Having established Hypotheses (H1), (H2), and (H3) we can invoke Theorem 4.1 to deduce the desired result.

Theorem 4.3. *Given an integer $s\geq 0$, if $X_0\neq 0$ and $X_1\in C^s([0,d])$ there exists a unique solution pair,* (3.11), *of the TM problem* (4.7) *satisfying*

$$\|U_\ell\|_{H^{s+1}} \leq C_U D^\ell, \quad \|W_\ell\|_{H^{s+3}} \leq C_W D^\ell, \quad \forall\, \ell\geq 0, \tag{4.9}$$

for any $D > C|X_1|_{C^s}$ where C_U and C_W are constants.

Remark 4.1. Before proceeding to our numerical investigations we emphasize what we have accomplished in Theorems 4.2 and 4.3, namely the *rigorous* demonstration of the *existence* and *uniqueness* of solutions to our model problems in both TE, (4.4), and TM polarizations, (4.7). In particular, this extends our results in [30] to the case of *nonlocal* models of two–dimensional materials.

5 Numerical results

We now discuss how the recursions outlined above can be implemented in a HOS scheme for simulating the surface scattered fields $\{U,W\}$. After describing the implementation we use our algorithm to simulate absorbance spectra of TM polarized plane waves incident upon a periodic grid of graphene ribbons as described in [10].

5.1 Implementation

A numerical implementation of our recursions is rather straightforward. To begin, we must truncate the HOPE expansions (3.11) after a finite number, L, of Taylor orders

$$\{U,W\} \approx \{U^L,W^L\} := \sum_{\ell=0}^{L} \{U_\ell,W_\ell\}(x)\delta^\ell,$$

which satisfy, in either TE or TM polarization, (3.12) up to perturbation order L. For this, in consideration of the quasiperiodic boundary conditions and our HOS philosophy [14, 40, 41], we utilize the finite Fourier representations

$$\{U_\ell,W_\ell\} \approx \{U_\ell^{N_x},W_\ell^{N_x}\} := \sum_{p=-N_x/2}^{N_x/2-1} \{\hat{U}_{\ell,p},\hat{W}_{\ell,p}\} e^{i\alpha_p x}, \quad 0 \le \ell \le L,$$

delivering

$$\{U,W\} \approx \{U^{L,N_x},W^{L,N_x}\} = \sum_{\ell=0}^{L} \sum_{p=-N_x/2}^{N_x/2-1} \{\hat{U}_{\ell,p},\hat{W}_{\ell,p}\} e^{i\alpha_p x}, \tag{5.1}$$

and, with a collocation approach, we simply demand that (3.12) be true at the equally–spaced gridpoints $x_j = (d/N_x)j$, $0 \le j \le N_x - 1$.

Due to the fact that the operators $\{G_0,J_0\}$ are Fourier multipliers, they can be readily applied in Fourier space after a Discrete Fourier Transform (DFT) which we accelerate by the Fast Fourier Transform (FFT) algorithm. Finally, we evaluate multiplication by the function $X_1(x)$ on the physical side, pointwise at the equally–spaced gridpoints x_j.

As with all perturbation schemes it is important to specify how the Taylor series in (5.1) are to be summed. On the one hand, "direct" Taylor summation seems natural, however, this method is limited to the *disk* of analyticity centered at the origin. In fact we have some rather explicit information about its size from the hypotheses of Theorem 4.1. This result demonstrates that, for any $0 \le \rho < 1$, we can expect convergence of the Taylor series for $\delta < \rho / B_V$ where

$$B_V \ge \max\{B_R, 2B_A, 4C_e C_A B_A\},$$

where we have selected $B_A = |X_1|_{C^s}$. In the results which follow we chose X_1 from (3.6) which is rather rough indicating that δ must be quite small for conventional Taylor summation.

However, it has been our experience that the actual domain of analyticity is much larger and may include the entire real axis (despite poles on the imaginary axis and elsewhere in the complex plane far from the real axis) [34]. One way to access this extended region of analyticity is the classical technique of Padé approximation [3] which has been used successfully for enhancing HOPS schemes in the past [33–35]. Padé approximation seeks to estimate the truncated Taylor series $f(\delta)=\sum_{\ell=0}^{L} f_\ell \delta^\ell$ by the rational function

$$\left[\frac{M}{N}\right](\delta) := \frac{a^M(\delta)}{b^N(\delta)} = \frac{\sum_{m=0}^{M} a_m \delta^m}{\sum_{n=0}^{N} b_n \delta^n}, \quad M+N=L,$$

and

$$\left[\frac{M}{N}\right](\delta) = f(\delta) + \mathcal{O}(\delta^{M+N+1});$$

well–known formulas for the coefficients $\{a_m, b_n\}$ can be found in [3]. These Padé approximants have stunning properties of enhanced convergence, and we point the interested reader to § 2.2 of [3] and the calculations in § 8.3 of [4] for a complete discussion.

5.2 Absorbance spectra

With an implementation of our algorithm we can now address questions of importance to practitioners. As a specific example, we consider the work of Goncalves, Dias, Bludov, and Peres [10] who studied the scattering of linear waves by arrays of graphene ribbons mounted between dielectric layers. More specifically we refer the reader to Figure 4 of [10] which shows the results of their investigations into the effect of the ribbon period on the frequency of a Graphene Surface Plasmon (GSP) excited by the configuration.

To generate this figure [10] focused upon TM polarization, set the physical parameters

$$\epsilon_u = 3, \quad \epsilon_w = 4, \quad E_F = 0.4 \text{ eV}, \quad \Gamma = 3.7 \text{ meV}, \tag{5.2}$$

and studied normal incidence so that $\theta = \alpha = 0$. The lateral period (which they denoted L) of the structure was varied among d=1,2,4,8 (in microns) while the width of the graphene in each period cell was set to $d/2$.

In the study of diffraction gratings, quantities of great physical interest are the efficiencies. Recalling the Rayleigh expansions, (3.8) and (3.10), and the definitions, (3.9), these are given by

$$e_{u,p} := \frac{\gamma_{u,p} \left|\hat{U}_p\right|^2}{\gamma_{u,0}}, \quad e_{w,p} := \frac{\gamma_{w,p} \left|\hat{W}_p\right|^2}{\gamma_{u,0}}.$$

With these we can define the reflectance, transmittance, and absorbance respectively as

$$R := \sum_{p \in \mathcal{U}_u} e_{u,p}, \quad T := \sum_{p \in \mathcal{U}_w} e_{w,p}, \quad A := 1 - R - \frac{\epsilon_u}{\epsilon_w} T;$$

we note that all–dielectric structures possess a principle of conservation of energy which mandates $A=0$. However, as graphene has noteworthy metallic properties, an indicator

DOI https://doi.org/10.4208/cicp.OA-2024-0241

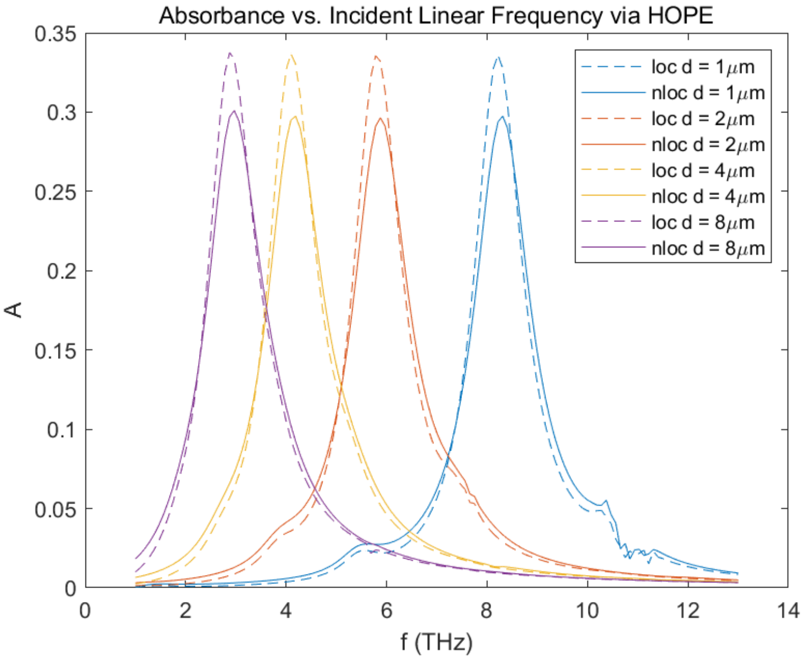

Figure 3: Plot of HOPE simulation of the absorbance spectra for normally incident plane–wave illumination of a periodic array of graphene ribbons with periodicity d mounted between two dielectrics. The physical parameters are specified in (5.2) and (5.3), and the numerical parameters were $N_x = 128$ and $L = 16$.

of a plasmonic response is given by a significant deviation of A from zero. Figure 4 of [10] is a plot of precisely this quantity, versus a range of illumination frequencies, for the four values of d mentioned above. In particular, we note significant peaks in A, the "absorbance spectra," of magnitude 0.35 in the vicinities of $\nu = 2,4,6,8$ THz for the values $d = 8,4,2,1$ microns, respectively. In subsequent work by Fallali, Low, Tamagnone, and Perruisseau–Carrier [8], this study was extended (with slightly different parameters) to include the nonlocal effects produced by the model we describe above.

With an implementation of our new recursions we attempted to recreate this work with both the local and nonlocal models. Our results, with the same physical parameters, (5.2), supplemented with

$$v_F = 1 \ \mu\text{m/s}, \quad \tau = 0.09 \text{ s}, \tag{5.3}$$

and numerical values $N_x = 128$ and $L = 16$, are displayed in Fig. 3 for $\delta = 1$. It is noteworthy that Padé approximation was *required* to achieve these results as Taylor summation diverged. We point out the remarkable *qualitative* agreement between the local results (dashed curves) and those of [10], which we take as evidence for the accuracy and utility of our approach. In addition, we point out the *shifted* solid curves generated by the nonlocal model, in particular the blueshift of the peaks to higher frequencies ν as also noted in [8].

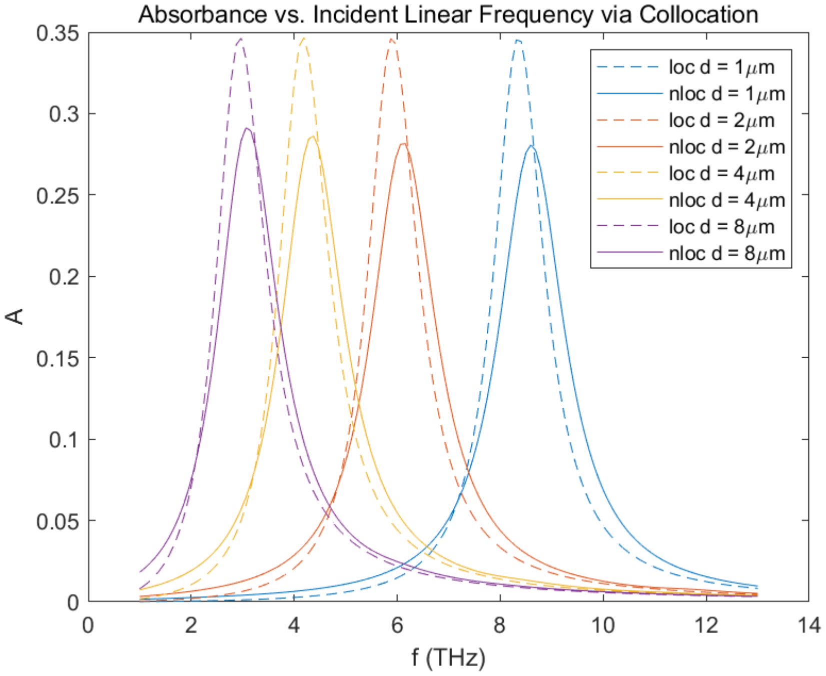

Figure 4: Plot of collocation simulation of the absorbance spectra for normally incident plane–wave illumination of a periodic array of graphene ribbons with periodicity d mounted between two dielectrics. The physical parameters are specified in (5.2) and (5.3), and the numerical parameter was $N_x = 128$.

Of course it is always useful to have additional validation, and for this we pondered the question of simply approximating the governing equations (3.7) with $\delta = 1$ using a collocation approach [14,40,41]: Expand the

$$\{U,W\} \approx \{U^{N_x},W^{N_x}\} = \sum_{p=-N_x/2}^{N_x/2-1} \{\hat{U}_p,\hat{W}_p\} e^{i\alpha_p x},$$

and demand that (3.7) be true at the gridpoints $x_j = (d/N_x)j$, $0 \leq j \leq N_x - 1$. We implemented this algorithm and achieved the results displayed in Fig. 4. Interestingly, the difference between these collocation results and our HOPE computations is largely negligible. (The "wiggles" seen in the high–frequency regime of Fig. 3 we attribute to the somewhat unstable nature of Padé summation which is sometimes observed [4].) Importantly, with non–optimized MATLAB™ [22] implementations of each algorithm, our new HOPE approach is nearly ten times faster than the collocation approach. For this reason we find our new algorithm to be quite compelling, though we intend to study this issue in a variety of settings in a forthcoming publication.

5.3 Validation and applicability

In light of the success reported in the previous section, one can ponder the veracity and limits of applicability of our new implementation. To address the former we revisit the calculations above with refined parameter choices to demonstrate that the results we produced are resilient. For the latter we conduct new investigations as various physical parameters are varied: The angle of incidence θ, the underlying dielectric constant, ϵ_w, and the patterning shape, $X_1(x)$.

We begin with Fig. 5 which revisited the computation that generated Fig. 3 (where $d=2\ \mu m$), save that only four incident frequencies were sampled: 3, 5, 7, and 9 THz. This figure shows the L^2–norm difference in the Dirichlet trace, U, between spatial discretizations N_x and $4N_x$, where N_x ranges among the even numbers between 4 and 64. With

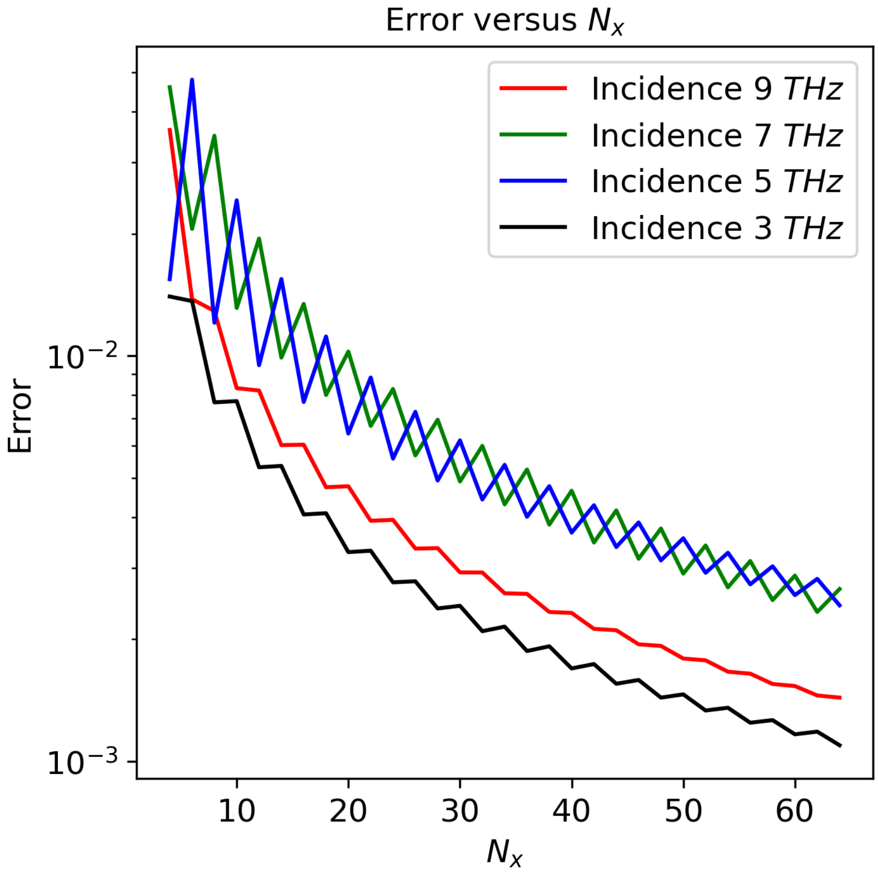

Figure 5: Plot of the L^2–norm difference in the Dirichlet trace, U, between spatial discretizations N_x and $4N_x$, in a HOPE simulation of the absorbance spectra for normally incident plane–wave illumination of a periodic array of graphene ribbons with periodicity d mounted between two dielectrics. The physical parameters are specified in (5.2) and (5.3), and the numerical parameters were $N_x=128$ and $L=16$.

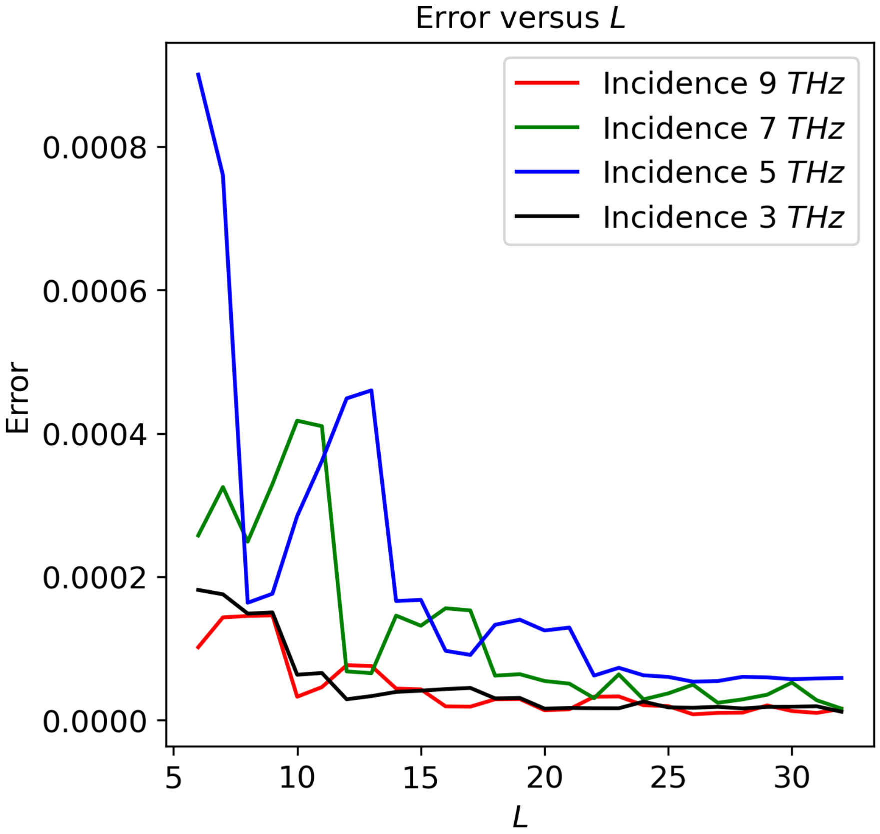

Figure 6: Plot of the L^2–norm difference in the Dirichlet trace, U, between Taylor truncations L and $2L$, in a HOPE simulation of the absorbance spectra for normally incident plane–wave illumination of a periodic array of graphene ribbons with periodicity d mounted between two dielectrics. The physical parameters are specified in (5.2) and (5.3), and the numerical parameters were $N_x = 128$ and $L = 16$.

only a small variance among the different f, the figure illustrates high accuracy as N_x is refined on this log–linear plot. There are small oscillations in the error as we varied adjacent values of N_x making the curves "zigzag" which we attribute to subtle aliasing error amplification/suppression. Despite this, increasing N_x generically led to great increases in accuracy.

We continued this study of the computation of Fig. 3 ($d = 2\ \mu m$ and $f \in \{3,5,7,9\}$ THz) by comparing the L^2–norm difference in the Dirichlet trace, U, between Taylor truncations L and $2L$; see Fig. 6. Our simulations showed that, despite small transient increases for certain f, the error generically dropped as L increased, particularly as L increased past 16. Once again, we take this as evidence of the steady and robust convergence of our algorithm even in these simulations featuring rather rough current envelope $X_1(x)$.

Moving to our second objective in this section, we persisted with our investigation of the structure with generated Fig. 3 ($d = 2\ \mu m$ and $f \in \{3,5,7,9\}$ THz). Fig. 7 shows our

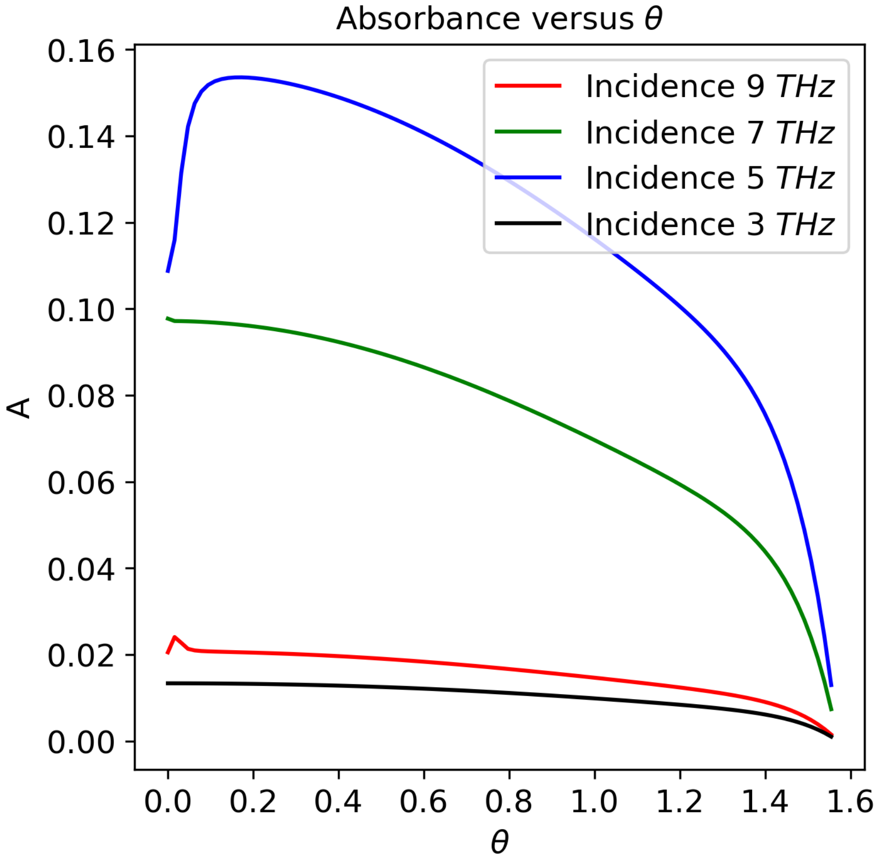

Figure 7: Plot of HOPE simulation of the absorbance spectra for plane–wave illumination with different incidence angles, θ, of a periodic array of graphene ribbons with periodicity d mounted between two dielectrics. The physical parameters are specified in (5.2) and (5.3), and the numerical parameters were $N_x = 128$ and $L = 16$.

simulation of absorbance spectra for different incidence angles θ. In this figure we notice a small increase in absorbance as θ increases from zero, but eventually it collapses to zero as θ moves to glancing incidence at $\theta = \pi/2$. In this case the incident field is parallel to the grating and does not illuminate the structure.

In Fig. 8 we display results of our investigation into the dependence of the absorbance on the permittivity of the lower layer, ϵ_w, as the permittivity of the upper layer, ϵ_u, is held fixed. Here we see different behavior based upon the frequency of illumination, however, we notice a nearly uniform smoothness in our results displaying the utility of our approach for these simulations.

To further study the performance of our implementation we considered a different envelope function $X_1(x)$. In contrast to our earlier investigations (see Fig. 3) featuring the rather rough envelope function, Fig. 2, which is merely continuous, we considered a

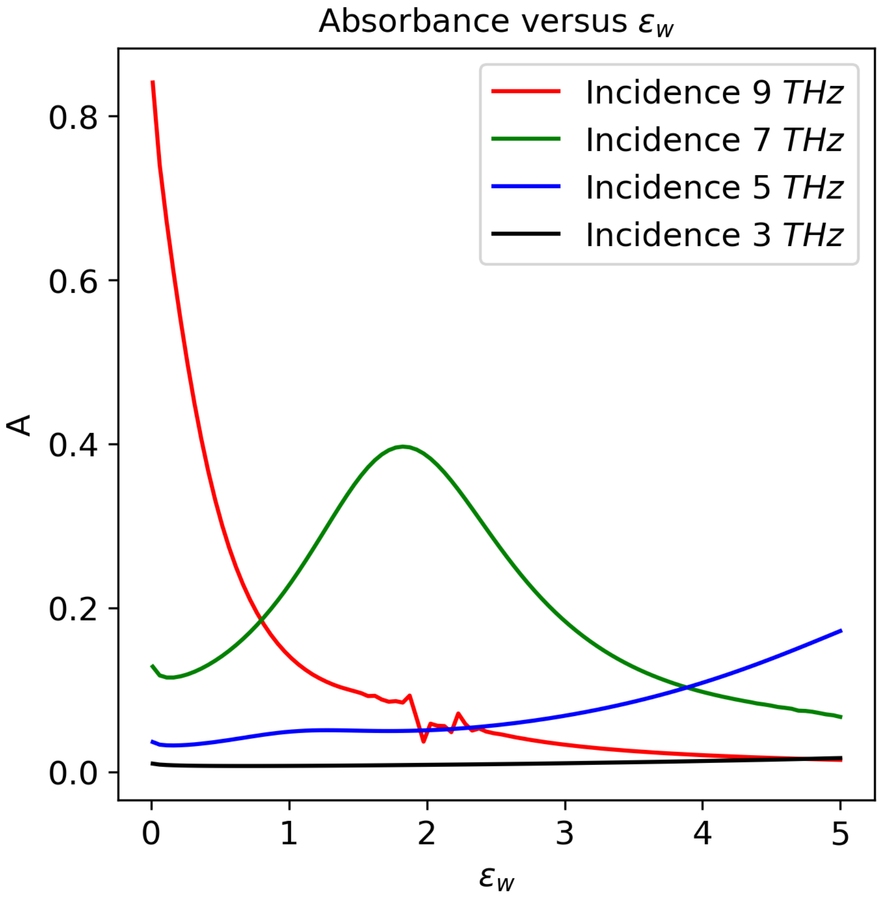

Figure 8: Plot of HOPE simulation of the absorbance spectra for normally incident plane–wave illumination of a periodic array of graphene ribbons with periodicity d mounted between two dielectrics with variable lower layer permittivity ϵ_w. The physical parameters are specified in (5.2) and (5.3), and the numerical parameters were $N_x = 128$ and $L = 16$.

smooth sinusoidal envelope

$$X_1(x) = -X_0 + \frac{1}{2}(1+\sin(2\pi x/d)). \tag{5.4}$$

With this new configuration we revisited our calculation of absorbance spectra which delivered Fig. 9. Here we see that the curves feature *multiple* peaks which are *not* well–separated. We feel that this result demonstrates how our algorithm can be effectively used to study the sensitive dependence of the absorbance on the envelope function.

Finally, in order to study the utility of Padé summation, we repeated the same simulation whose results are depicted in Fig. 3, with Taylor summation replacing the Padé technique. The striking results are shown in Fig. 10 which shows that not only do the spectra take on unphysical negative numbers, they are also ridiculously large in magni-

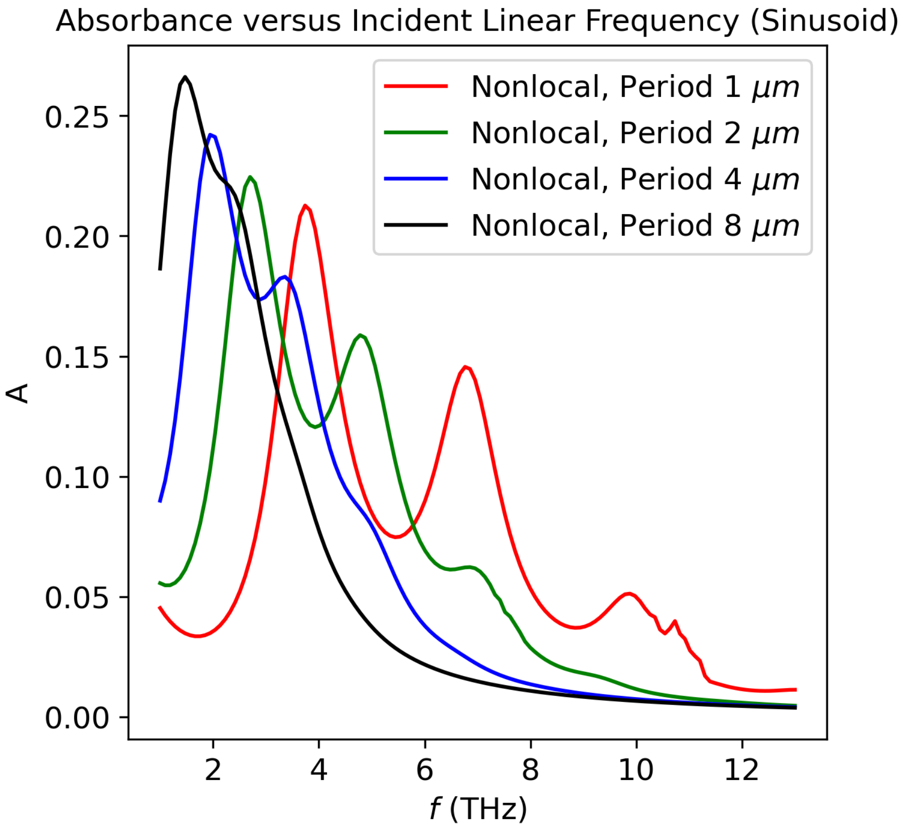

Figure 9: Plot of HOPE simulation of the absorbance spectra for normally incident plane–wave illumination of a periodic array of graphene ribbons, shaped by a sinusoidal profile (5.4) with periodicity d mounted between two dielectrics. The physical parameters are specified in (5.2) and (5.3), and the numerical parameters were $N_x = 128$ and $L = 16$.

tude! For this configuration we admit the absolute necessity of Padé summation in order to realize useful simulation results.

6 Conclusions

In this paper we have described the extension of our High–Order Perturbation of Envelopes (HOPE) algorithm from doubly layered media with interfacial graphene (or other two–dimensional materials) to the situation where non–local effects are important. This was highly non–trivial as the modification to the surface current which models such materials introduces higher derivative terms and mandates the use of different Sobolev spaces and enhanced linear estimates. In addition, we reported on a novel numerical implementation with supporting numerics to verify its accuracy and utility. Our devel-

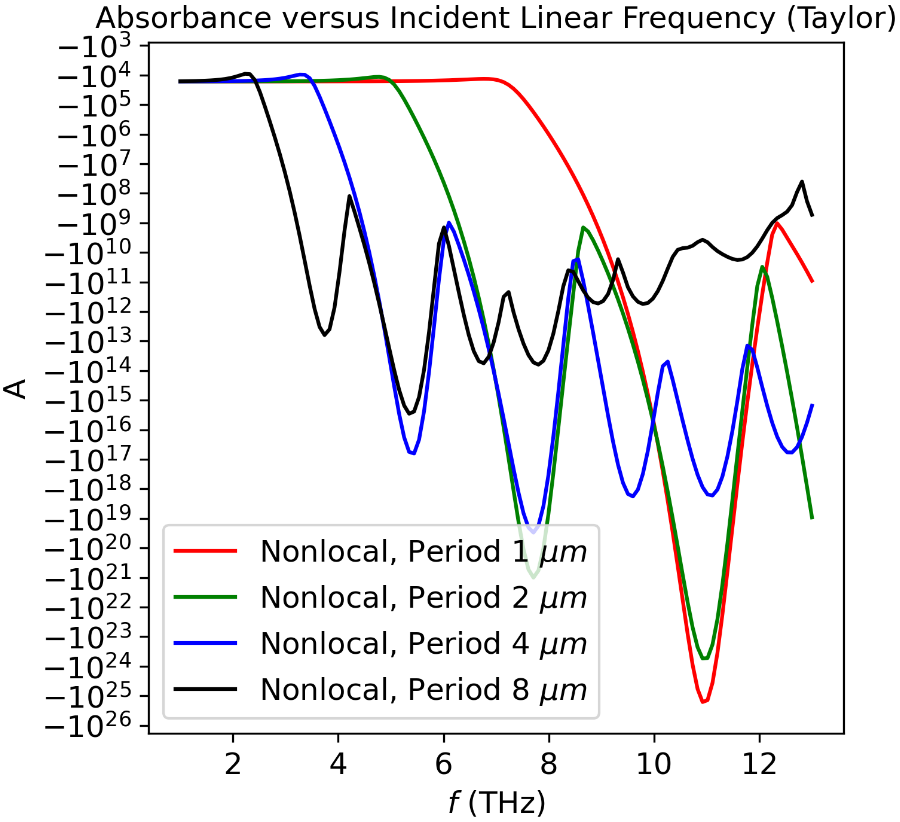

Figure 10: Plot of HOPE simulation of the absorbance spectra for normally incident plane–wave illumination of a periodic array of graphene ribbons with periodicity d mounted between two dielectrics. The physical parameters are specified in (5.2) and (5.3), and the numerical parameters were $N_x=128$ and $L=16$. Perturbation series evaluated with direct Taylor summation.

opments naturally point the way to further enhancements, in particular the possibility of simulating periodically *corrugated* sheets of graphene, e.g., shaped by $z=\varepsilon f(x)$. Regarding this, the formulation (3.4) is still valid and one merely needs to focus on the dependence of the DNOs, G and J, on ε and f. Given our previous work on analyticity properties of these operators [36] it seems that an analogous theory and implementation can be achieved, and we fully intend to investigate this possibility.

Acknowledgments

D.P.N. gratefully acknowledges support from the National Science Foundation through grant No. DMS–2111283.

References

[1] Tilo Arens. *Scattering by Biperiodic Layered Media: The Integral Equation Approach*. Habilitationsschrift, Karlsruhe Institute of Technology, 2009.

[2] Y. Bludov, A. Ferreira, N. Peres, and M. Vasilevskiy. A primer on surface plasmon–polaritons in graphene. *International Journal of Modern Physics B*, 27:1341001, 2013.

[3] George A. Baker, Jr. and Peter Graves-Morris. *Padé Approximants*. Cambridge University Press, Cambridge, second edition, 1996.

[4] Carl M. Bender and Steven A. Orszag. *Advanced Mathematical Methods for Scientists and Engineers*. McGraw-Hill Book Co., New York, 1978. International Series in Pure and Applied Mathematics.

[5] COMSOL. *COMSOL Multiphysics Reference Manual*. COMSOL, Inc., Stockholm, Sweden, 2024.

[6] D. Correas-Serrano, J. S. Gomez-Diaz, M. Tymchenko, and A. Alù. Nonlocal response of hyperbolic metasurfaces. *Opt. Express*, 23(23):29434–29448, Nov 2015.

[7] Lawrence C. Evans. *Partial Differential Equations*. American Mathematical Society, Providence, RI, second edition, 2010.

[8] A. Fallahi, T. Low, M. Tamagnone, and J. Perruisseau-Carrier. Nonlocal electromagnetic response of graphene nanostructures. *Physical Review B Rapid*, 91:121405, 2015.

[9] B. Gallinet, J. Butet, and O. J. F. Martin. Numerical methods for nanophotonics: Standard problems and future challenges. *Laser and Photonics Reviews*, 9:577–603, 2015.

[10] P. A. D. Goncalves, E. J. C. Dias, Y. V. Bludov, and N. M. R. Peres. Modeling the excitation of graphene plasmons in periodic grids of graphene ribbons: An analytical approach. *Physical Review B*, 94:195421, 2016.

[11] A. Geim. Graphene: Status and prospects. *Science*, 324:1530–1534, 2009.

[12] A. Geim. Random walk to graphene (nobel lecture). *Angewandte Chemie International Edition*, 50:6966–6985, 2011.

[13] A. Geim and K. Novoselov. The rise of graphene. *Nature Materials*, 6:183–191, 2007.

[14] D. Gottlieb and S. A. Orszag. *Numerical analysis of spectral methods: Theory and applications*. Society for Industrial and Applied Mathematics, Philadelphia, Pa., 1977. CBMS-NSF Regional Conference Series in Applied Mathematics, No. 26.

[15] P. A. D. Goncalves and N. M. R. Peres. *An Introduction to Graphene Plasmonics*. World Scientific, Singapore, 2016.

[16] Y. Hong and D. P. Nicholls. On the consistent choice of effective permittivity and effective conductivity for modeling graphene. *Journal of the Optical Society of America, A*, 38:1511–1520, 2021.

[17] Marinko Jablan, Hrvoje Buljan, and Marin Soljačić. Plasmonics in graphene at infrared frequencies. *Phys. Rev. B*, 80:245435, Dec 2009.

[18] Jianming Jin. *The Finite Element Method in Electromagnetics*. Wiley-Interscience [John Wiley & Sons], New York, second edition, 2002.

[19] Marinko Jablan, Marin Soljačić, and Hrvoje Buljan. Plasmons in graphene: Fundamental properties and potential applications. *Proceedings of the IEEE*, 101(7):1689–1704, 2013.

[20] Pavel Kwiecien, Milan Burda, and Ivan Richter. Nonlocal Fourier modal method for analyzing nonlocal plasmonic periodic nanostructures. *J. Opt. Soc. Am. B*, 40(3):491–500, Mar 2023.

[21] Wenyue Li, Yanfen Zhou, Yuhao Wang, Ying Li, Liang Jiang, Jianwei Ma, and Shaojuan Chen. Highly stretchable and sensitive SBS/graphene composite fiber for strain sensors.

Macromolecular Materials and Engineering, 305(3):1900736, 2020.

[22] MATLAB. *MATLAB version 24.1.0.2537033 (R2024a)*. The MathWorks Inc., Natick, Massachusetts, 2024.

[23] Tiago A. Morgado and Mário G. Silveirinha. Nonlocal effects and enhanced nonreciprocity in current-driven graphene systems. *Phys. Rev. B*, 102:075102, Aug 2020.

[24] Graphene: Latest Research and Reviews. World Wide Web Site, August 2024. http://www.nature.com/subjects/graphene.

[25] Lina Nie, Chong Yang Chuah, Tae-Hyun Bae, and Jong-Min Lee. Graphene-based advanced membrane applications in organic solvent nanofiltration. *Advanced Functional Materials*, 31:2006949, 2021.

[26] K. S. Novoselov, A. K. Geim, S. V. Morozov, D. Jiang, Y. Zhang, S. V. Dubonos, I. V. Grigorieva, and A. A. Firsov. Electric field effect in atomically thin carbon films. *Science*, 306(5696):666–669, 2004.

[27] D. P. Nicholls. Three–dimensional acoustic scattering by layered media: A novel surface formulation with operator expansions implementation. *Proceedings of the Royal Society of London, A*, 468:731–758, 2012.

[28] D. P. Nicholls. On analyticity of linear waves scattered by a layered medium. *Journal of Differential Equations*, 263(8):5042–5089, 2017.

[29] D. P. Nicholls. Numerical simulation of grating structures incorporating two–dimensional materials: A high–order perturbation of surfaces framework. *SIAM Journal on Applied Mathematics*, 78(1):19–44, 2018.

[30] D. P. Nicholls. High–order spectral simulation of graphene ribbons. *Comm. Comput. Phys.*, 26:1575–1596, 2019.

[31] D. P. Nicholls, S.-H. Oh, T. W. Johnson, and F. Reitich. Launching surface plasmon waves via vanishingly small periodic gratings. *Journal of the Optical Society of America, A*, 33(3):276–285, 2016.

[32] K. Novoselov. Graphene: Materials in the flatland (nobel lecture). *Angewandte Chemie International Edition*, 50:6986–7002, 2011.

[33] D. P. Nicholls and F. Reitich. A new approach to analyticity of Dirichlet-Neumann operators. *Proc. Roy. Soc. Edinburgh Sect. A*, 131(6):1411–1433, 2001.

[34] D. P. Nicholls and F. Reitich. Analytic continuation of Dirichlet-Neumann operators. *Numer. Math.*, 94(1):107–146, 2003.

[35] D. P. Nicholls and F. Reitich. Shape deformations in rough surface scattering: Improved algorithms. *J. Opt. Soc. Am. A*, 21(4):606–621, 2004.

[36] D. P. Nicholls and J. Shen. A rigorous numerical analysis of the transformed field expansion method. *SIAM Journal on Numerical Analysis*, 47(4):2708–2734, 2009.

[37] A.G. Olabi, Mohammad Ali Abdelkareem, Tabbi Wilberforce, and Enas Taha Sayed. Application of graphene in energy storage device — a review. *Renewable and Sustainable Energy Reviews*, 135:110026, 2021.

[38] R. Petit, editor. *Electromagnetic Theory of Gratings*. Springer-Verlag, Berlin, 1980.

[39] Saijie Song, He Shen, Yuli Wang, Xiaohong Chu, Jing Xie, Ninglin Zhou, and Jian Shen. Biomedical application of graphene: From drug delivery, tumor therapy, to theranostics. *Colloids and Surfaces B: Biointerfaces*, 185:110596, 2020.

[40] Jie Shen and Tao Tang. *Spectral and High-Order Methods with Applications*, volume 3 of *Mathematics Monograph Series*. Science Press Beijing, Beijing, 2006.

[41] Jie Shen, Tao Tang, and Li-Lian Wang. *Spectral Methods*, volume 41 of *Springer Series in Computational Mathematics*. Springer, Heidelberg, 2011. Algorithms, analysis and applications.

[42] He Shen, Liming Zhang, Min Liu, and Zhijun Zhang. Biomedical applications of graphene. *Theranostics*, 2:283–294, 2012.

[43] Allen Taflove and Susan C. Hagness. *Computational Electrodynamics: The Finite-Difference Time-Domain Method*. Artech House, Inc., Boston, MA, second edition, 2000.

[44] Pochi Yeh. *Optical Waves in Layered Media*, volume 61. Wiley-Interscience, 2005.

[45] Shunshun Zhu, Baojun Wang, and Bin Guo. Dispersion relation of graphene surface plasmon by using a quantum hydrodynamic model. *Superlattices and Microstructures*, 142:106516, 2020.